A Letters Journal Exploring the Frontiers of Physics

May 2011

EPL, **94** (2011) 47002
doi: 10.1209/0295-5075/94/47002

www.epljournal.org

Transport response of carbon-based resonant cavities under time-dependent potential and magnetic fields

C. G. Rocha[1], M. Pacheco[2], L. E. F. Foa Torres[3], G. Cuniberti[1] and A. Latgé[4(a)]

[1] *Institute for Materials Science and Max Bergmannn Center of Biomaterials, Dresden University of Technology D-01062 Dresden, Germany, EU*
[2] *Departamento de Física, Universidad Federico Santa María - Valparaíso, Chile*
[3] *IFEG (CONICET) and FaMAF, Universidad Nacional de Córdoba, Ciudad Universitaria 5000 Córdoba, Argentina*
[4] *Instituto de Física, Universidade Federal Fluminense s/n - 24210-340 Niterói-RJ, Brazil*

received 11 March 2011; accepted in final form 6 April 2011
published online 4 May 2011

PACS 72.80.Vp – Electronic transport in graphene
PACS 73.23.-b – Electronic transport in mesoscopic systems

Abstract – Here we report theoretical transport calculations on carbon-based nanomaterials used as resonator cavities under the effects of a time-dependent field. A magnetic field is considered as an extra modulator tool, able to encode binary ON or OFF transmission states on the quantum systems. Regular either complex conductance Fabry-Pérot patterns mapped onto gate *vs.* bias voltage diagrams can be revealed depending on the set of parameters used on the simulations (amplitude and frequency of the ac field and magnetic-field intensity). We discuss the interplay between the effects on the resonant cavity conductance, caused by the presence of an ac gate plate, which tends to delocalize the electronic wave functions, and an external magnetic field that oppositely localizes the electrons.

Introduction. – Carbon nanotubes (CNTs) and graphene nanoribbons (GNRs) have been intensively studied due to their outstanding electrical properties [1,2] that can render ultimately technological applications [3,4] such as transistors, sensors and interconnects [5,6]. In contrast to usual molecular electronics experiments revealing Coulomb blockade phenomena, the concrete ability in achieving almost transparent contacts between the carbon-based transmission channel and electrodes favors the ballistic transport. A signature of such transport regime is marked by the observation of regular Fabry-Pérot (FP) oscillations mapped onto gate *vs.* bias voltage diagrams [7]. Recent experiments [8] conducted on large CNTs (≈ 5 nm of radio and 220 nm of extension) exposed to high magnetic-field regime, indicate that FP-like conductance oscillations can be effectively modulated as the intensity of the field varies. Importantly, characteristic scale lengths such as the Landau radii (l_B) dictate the appearance of Landau levels in the diagrams. Whenever l_B is lesser than the tube's extension, Landau levels are generated. Moreover, magnetic fields may also induce metal-insulator transitions in CNTs, offering an efficient way of inducing bandgap engineering at nanoscale [9–12].

Another possibility of controlling the electronic transmission of nanomaterials is the use of time-dependent fields [13]. Recent studies targeting the use of ac fields in carbon-based materials [14–16] shed light on this growing research area, often overshadowed by studies considering external fields in the stationary regime. Previous works have considered the effect of ac gate acting on CNTs and GNRs as a mean of achieving full control of the conductance patterns [14,17]. The results have pointed to several possibilities of tuning the conductance profiles which range from suppression, phase change of the oscillations, up to robust behaviours observed even in the presence of highly intensive fields. In particular, the transport properties of the systems can be dragged towards the robustness while the driving frequency ω fulfills the stroboscopic condition: $\hbar\omega = n\Delta$, being Δ the energy level spacing of the resonant cavity, ω the ac-field frequency, and n an integer number which mimics the well-known wagon-wheel effect, now held in the quantum domain. In order to enhance the viability in incorporating such ac building-block components into

(a) E-mail: latge@if.uff.br

real nanodevices, it is of relevance to drive the system's properties beyond these possible scenarios. Different transport states can be unfolded combining the influences generated by time-dependent excitations with external magnetic fields. In this sense, this work investigates the effects of the interplay between a static magnetic field and an ac gate acting on biterminal architectures where CNTs or GNRs appear as the main transmission channel. We demonstrated that the homogeneous field induces prominent conduction gaps on the gate *vs.* bias diagrams. These results highlight an alternative way of coexistence of both suppression state and regular FP oscillations, for instance, without the need of changing the frequency of the ac field.

Theoretical model. – The full system, composed of a central scattering region of length L connected to semi-infinite leads, is modeled by a single π-band tight-binding approach within a noninteracting picture. The Hamiltonian of the system is written in a real-space basis and parameters such as on-site energy (ϵ_o) and nearest-neighbour hopping elements (γ_o) must be defined. In general for a pristine carbon-based structure without any perturbation, $\epsilon_o = 0$ and $\gamma_o = 2.7\,\mathrm{eV}$. To simulate the quasi-transparent contacts between electrodes and central part, we define an additional hopping element which is slightly smaller than the carbon-carbon hopping parameter, *i.e.*, $\gamma' = 0.7\gamma_o$. This choice was shown to provide conductance profiles in good agreement with experimental data extracted from carbon nanotube-based resonators [7,18]. The action of an external homogeneous magnetic field B can be incorporated in the description following Peierls phase approximation where the hopping elements are modified by a phase factor that depends on the B intensity [9–12]. For the particular situation of B applied perpendicularly to the axial direction of a carbon nanotube, one can define an undimensional parameter able to control the strength of the field, $\nu_B = C/2\pi\ell_B$, being C the circumferential length of the tube and $\ell_B = \sqrt{\hbar/eB}$ the Landau radii. The B intensity is then given in tesla as $B = 25.98 \times 10^{-15}(\nu_B/C)^2$, leading to experimentally feasible quantities [8,19]: for a (30,0) CNTs and ν_B varying from 0.2 to 0.4 the field intensity changes approximately from 19 to 70 T. Likely, for B flowing perpendicularly through a graphene nanoribbon, one defines a parameter $\nu_B = \phi/\phi_o$ written in terms of the magnetic flux, $\phi = BA$ threading a single hexagon of area $A = 3\sqrt{3}a^2/2$ and $\phi_o = h/e$ being the quantum magnetic flux. Under dc conditions, the conductance of the system can be calculated adopting the Landauer formalism $\mathbf{G}(\epsilon) = 2e^2/hT(\epsilon)$, in which the transmission function $T(\epsilon)$ is written in terms of electronic propagators [20] as $T(\epsilon) = Tr[\Gamma_L G_C^r(\epsilon)\Gamma_R G_C^a(\epsilon)]$, with $G_C^{r(a)}$ being the retarded (advanced) Green function of the FP cavity and $\Gamma_{R(L)}$ the coupling energy between right (left) lead and the conductor, which is given in terms of the lead self-energy. We adopt standard real-space decimation procedures to obtain the surface propagators that represent the electronic contribution from the leads and the Green function associated to the central region [11,21].

A different theoretical framework has to be followed in order to include the influence of time-dependent excitations in the description. We consider the presence of an homogeneous time-dependent gate that changes the on-site energy of the atoms located on the central region as, $\epsilon_C(t) = \epsilon_C(0) + V_{ac}\cos(\omega t)$, being V_{ac} and ω the amplitude and frequency of the ac signal, respectively. Solving the time-dependent Schrödinger equation for such harmonic potential [13,22,23], it is possible to show that the time-averaged spectral function, $\langle A\rangle$, can be written in terms of the density of states of the system when no ac signal is applied ($\rho_o(E)$), standing as

$$\langle A\rangle = \sum_{m=-\infty}^{\infty} J_m^2\left(\frac{eV_{ac}}{\hbar\omega}\right)\rho_o(E + m\hbar\omega), \qquad (1)$$

where J_m is the m-th order Bessel function of the first kind and E is the energy [24]. This equation can be physically interpreted as follows: photon absorption ($m > 0$) and emission ($m < 0$) processes are described as creating an effective electron density of states at energies shifted by multiples of the photon energy, $\pm m\hbar\omega$, with a probability given by the Bessel factor $J_m^2(eV_{ac}/\hbar\omega)$. Likely, transport quantities such as dc current and conductance of a transmission channel under the effects of such homogenous ac field can be obtained following the same arguments used to compute the spectral function. Landauer formalism can still be adopted taking into account the modifications on the transition probabilities and the energy shifts due to absorption/emission of photons. Such theoretical treatment, known as Tie-Gordon formalism, works rather well when charge accumulation at the interfaces may be neglected [25].

In what follows we present our results for two probing carbon-based systems (CNTs and GNRs), chosen to be exposed to ac-gate signals and an external field B, applied perpendicularly to their transmission direction. A complete information about their conducting properties is obtained performing a fine scan of the dc voltages (bias and gate) to generate conductance contour plots. We investigate how the conductance pattern maps are sensitive to ac gating and magnetic fields.

Results. – Results obtained under dc conditions are taken as reference for our analysis, to distinguish the effects caused by an ac gate on the selected systems. A finite (6,0) metallic nanotube of length $L \approx 43.3$ nm (approximately 100 unit cells in size) is placed between two terminals working as coherent electron waveguide. Bias (V_{bias}) and gate (V_{gate}) voltages are varied simultaneously and, for each voltage intensity, the conductance ($\mathbf{G}$) of the system is calculated, and given in terms of the quantum conductance, $G_o = 2e^2/h$. Bias intensity controls the chemical potential of the electrodes while the gate modulates the position of the Fermi level in the interferometer.

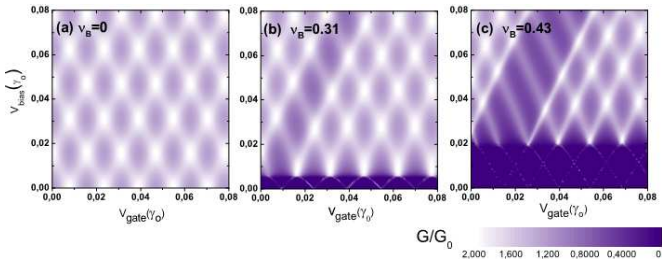

Fig. 1: (Color online) Contour plots of the conductance mapped onto $V_{bias} \times V_{gate}$ space phase for a (6,0) CNT resonator of length $L \approx 43.3\,\text{nm}$ operating at dc regime. Each panel corresponds to distinct B values given by: (a) $\nu_B = 0$, (b) $\nu_B = 0.31$, and (c) $\nu_B = 0.43$. Dark and bright colors represent lower and higher conductance values, respectively.

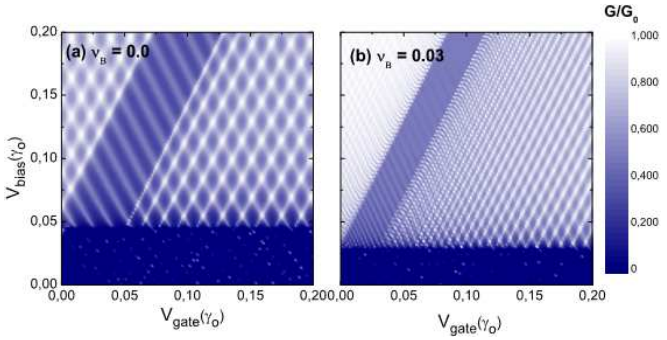

Fig. 2: (Color online) Contour plots of the conductance mapped onto $V_{bias} \times V_{gate}$ space phase obtained for a 14-AGNR resonator of length $L \approx 42.3$ nm operating at dc regime. The left (right) panel corresponds to $\nu = 0.0$ ($\nu_B = 0.03$). Dark and bright colors represent lower and higher conductance values, respectively.

The dc conductance diagrams are shown in fig. 1 considering distinct B intensities: (a) $\nu_B = 0$, (b) $\nu_B = 0.31$, and (c) $\nu_B = 0.43$. One can notice the formation of the characteristic FP diagrams where the transmission oscillates between maximum and minimum values. For null B (panel (a)), the maximum size of the diamonds with respect to the variation of V_{gate} corresponds exactly to the energy level spacing (Δ) of the finite conductor, defined as $\Delta \approx 3a_{cc}\gamma_o\pi/2L$, where $a_{cc} = 1.44\,\text{Å}$ is the carbon-carbon distance. In other words, the energy dispersion of infinitely long metallic tubes evidences a linear relation with the wave number at low-energy range. This guarantees that its energy spectrum is regularly discretized for a cavity of finite length. Since the device operates at near-perfect Ohmic regime, the gate voltage works like an energy spectrum "reader" of the resonator.

As expected, such a regular pattern modifies when an applied magnetic field is taken into account. At a critical field value a metallic tube suffers from a metal-insulator transition, leading to changes in the related electronic structure of the system. Modification of the electronic character of a (6,0) CNT can be clearly seen in panels (b) and (c) of fig. 1. Pronounced conductance gaps are formed (along the V_{bias} axis at $V_{gate} = 0$), corresponding exactly to the energy gap of the tube due to the magnetic field. Once V_{bias} overcomes the bandgap size, the FP pattern is recovered, however a line composed of elongated diamonds appears in the diagrams. The symmetric feature of the energy spectrum, characterized previously by an unique energy length scale (Δ) is broken when B transforms the system into semiconductor. Some reminiscence of the FP oscillations appears inside the conduction gap as V_{gate} is varied. This corresponds to situations where the bias voltage still lays on the bandgap range, however V_{gate} drags available energy states into such active bias windows. Comparing the diagram obtained at $B = 0$ with the ones where $\nu_B \neq 0$, one can say that they remarkably resemble each other except for the existence of conductance gaps and regions containing deformed diamonds. In particular, in fig. 1(c), B is strong enough to open a prominent conduction gap in the diagram which persists until V_{bias} reaches $\approx 0.02\gamma_o$, independently of the gate voltage value. Above this critical value, the FP pattern is recovered, although exhibiting deformations associated with the magnetic field. Therefore, a FP-semiconductor transition can be tuned by the applied bias.

A similar discussion can be employed for the case of a 14-AGNR resonator with a length of $L \approx 42.3\,\text{nm}$ and, consequently, an energy level spacing of $\Delta = 0.016\gamma_o$. When no magnetic flux is present, the semiconducting character of the armchair ribbon is already detected, as seen in fig. 2(a). At $V_{gate} = 0$, we determine an energy gap of $E_g = V_{bias}^{max} \approx 0.05\gamma_o$. As a certain amount of magnetic flux threads the ribbon sheet, the bandgap decreases (see panel (b) for $\nu_B = 0.03$) in accordance with magnetotransport experiments in graphene nanoribbons [19]. The presence of B leads the electronic character of the system closer to metallicity. For the particular case of the studied armchair ribbon with 14 atoms along its width, we determined that the energy gap can be closed totally at $\nu_B \approx 0.07$. For B values beyond this value, the gap is recovered and increases as the field gets stronger. Although ribbons and tubes are composed of carbon atoms disposed on hexagonal nets, their transmission profiles can be rather different since their transport response with respect to B is dictated by the material shape configuration (cylinder or flat ribbon) with the direction of the field (perpendicular to the tubes axis or to the ribbons plane). Distinct Peierls phase elements are calculated from such material/magnetic-field arrangements, leading to intriguing interference patterns when we compare the results of these two carbon structures under the influence of external magnetic fields.

The FP patterns can be efficiently tuned with the aid of two competing effects generated by applying magnetic and ac fields simultaneously: i) the ac modulation tends to delocalize the electronic wave functions whereas ii) B acts as an extra source of confinement for the

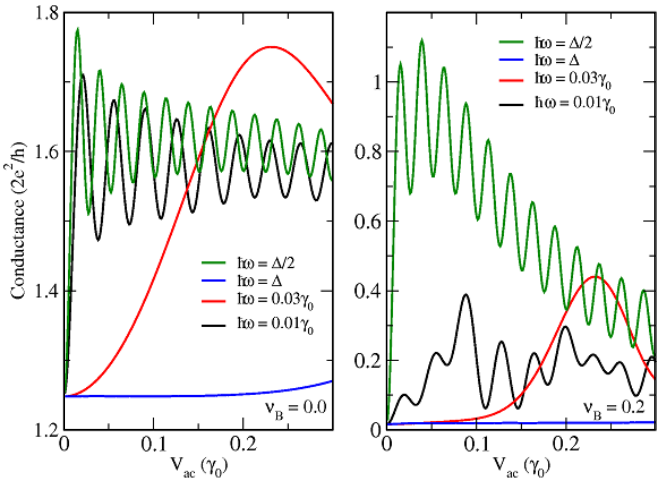

Fig. 3: (Color online) Conductance of a (6,0) CNT as a function of the ac potential amplitude, for different values of the ac frequency, and for (a) $\nu = 0$ and (b) $\nu = 0.2$. All curves are calculated at $V_{bias} = V_{gate} = 0$ and the energy level spacing is given by $\Delta = 0.015\gamma_o$.

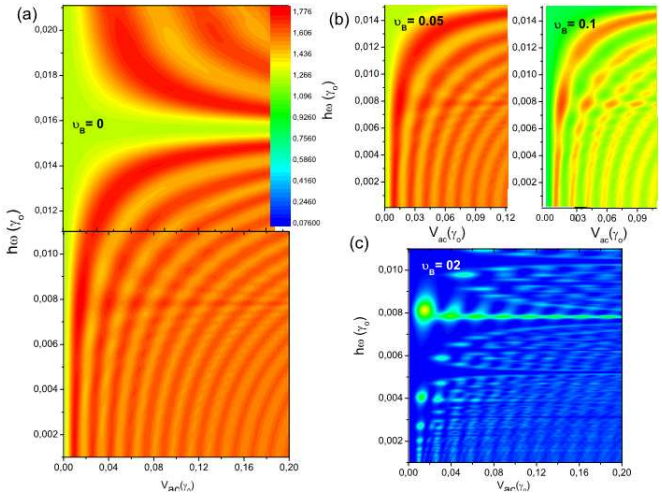

Fig. 4: (Color online) Conductance contour plot as a function of the ac amplitude (V_{ac}) and frequency ($\hbar\omega$) obtained for a (6,0) CNT under $V_{gate} = V_{bias} = 0$. Different panels correspond to: (a) $\nu_B = 0$, (b) $\nu_B = 0.05$ and 0.1, and (c) $\nu_B = 0.2$.

electronic states. The interplay between these two perturbing agents certainly leads the system to experience a variety of physical scenarios. In fig. 3, we show the conductance dependence of a (6,0) CNT with respect to the amplitude of the ac field (V_{ac}) while fixing the driving frequency at certain values. For two particular frequencies displayed on panel (a) ($\hbar\omega = 0.01\gamma_o$ and $\hbar\omega = \Delta/2$), the conductance oscillates as a function of V_{ac} but the periodic behaviour gradually damps at a certain conductance value as the amplitude intensity increases. This can be explained assuming adiabatic transport regime for the ac transmission where $\hbar\omega \ll \Delta$ [17]. Indeed, we proved that the transport behaviour of the metallic CNT can be effectively modulated by ac potentials; depending on the $\{V_{ac}, \hbar\omega\}$ parameters, the conductance can develop damped oscillations or reach an stable transmission state whenever $\hbar\omega$ matches with integer multiples of the energy level spacing. The conductance is severely reduced in all displayed curves for $\nu_B = 0.2$ in relation to the case of $\nu_B = 0.0$, evidencing that the magnetic field disables several conducting channels. At $V_{ac} = 0$, no transmission occurs in the channel but, as the ac gate is switched on, conducting states can become available due to the ac-induced splitting of levels given by $E \to E \pm m\hbar\omega$. Depending on the driving frequency and the transition probabilities that rule the absorption and emission of photons, additional states can be generated on the energy spectrum, contributing, though, to the ac transport. In particular, for $\hbar\omega = \Delta/2$, the number of active channels can reach approximately one at low oscillating amplitudes. Subsequently, the transmission reduces since the photon excitation probabilities, written in terms of Bessel functions, $J_m(x)$, decay oscillating as $x = eV_{ac}/\hbar\Delta$ increases.

In general, the regular damped oscillations (fig. 3(a)) are fully disturbed as B is considered. The sequence of equally spaced energy levels of the system is cut off by the opening of the bandgap. The gap energy now enters as an additional scale length (besides the spacing Δ) that also plays an important role in the ac transport response. Nevertheless, the inclusion of B seems not to interfere on the stability of the stroboscopic state since the original semiconducting behaviour of the tube is totally recovered when $\hbar\omega = \Delta$. The (mis)matching between these two energy scales can dictate the appearance of photonic states on the energy gap window and so the conductance in such robust state can also be finely adjusted.

Conductance patterns of the nanotube resonator, for distinct combinations of V_{ac} and $\hbar\omega$, are shown in the contour plots of fig. 4. Red and blue colors correspond to maximum and minimum conductance values, respectively. The well-defined FP oscillations together with the stroboscopic state where the patterns are insensitive to the ac field can be observed in panel (a) for $\nu_B = 0.0$. As the B intensity gets pronounced, such oscillations are gradually washed out. For $\nu_B = 0.2$, only residual transmissions can be detected at certain values of $\hbar\omega$ that correspond exactly to semi-multiples of the characteristic energy scale Δ. In particular for $\hbar\omega = \Delta/2 \approx 0.008\gamma_o$, a robust transmission state can be observed. A simple explanation for such persistent feature is raised in terms of a quantized energy spectrum that changes as photons are absorbed or emitted, as the ac signal is applied. For instance, the photon-induced states can be divided in two distinct categories: i) even excitations, corresponding to $m = 0,\ 2,\ 4,\ \ldots$ and ii) odd modes given by $m = 1,\ 3,\ 5,\ \ldots$. When $\hbar\omega = \Delta/2$, the even-order excitations will generate photonic states at $E = 0, \pm\Delta, \pm 2\Delta, \pm 3\Delta, \ldots$

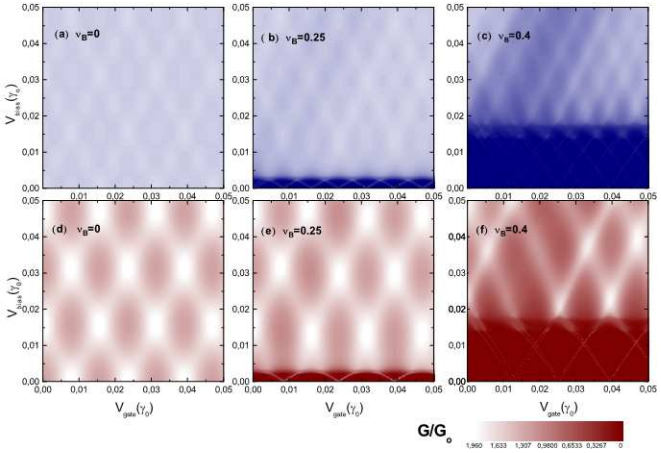

Fig. 5: (Color online) 2D FP conductance diagram, $V_{bias} \times V_{gate}$ of a (6,0) CNT, in the absence of magnetic flux ((a) and (d)) and for $\nu_B = 0.25$ ((b) and (e)), and $\nu_B = 0.40$ ((c) and (f)). In upper and lower diagrams $V_{ac} = 0.01\gamma_o$ and the photon frequencies are $\hbar\omega = \Delta/2$ and Δ, respectively.

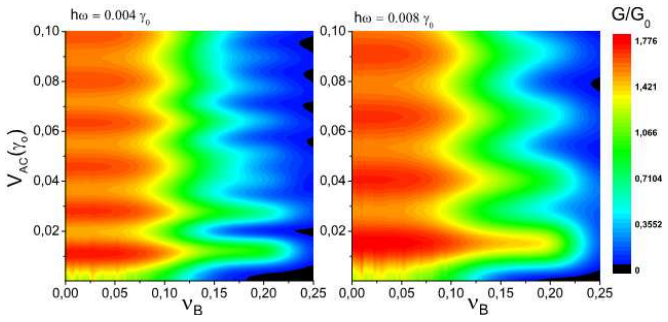

Fig. 6: (Color online) 2D conductance diagram calculated at the Fermi energy as a function of the amplitude of the ac potential and the magnetic-field intensity ($V_{bias} = V_{gate} = 0$).

which are commensurate to the energy level spacing. If only the contributions of such excitations are considered in the transmission, the system would behave as it was standing on a wagon-wheel condition where its intrinsic semiconducting character is recovered. However, the excitations of odd order split the energy states into intermediate positions such as $E = 0, \pm\Delta/2, \pm 3\Delta/2, \ldots$. Even in the presence of intensive B, the contribution coming from such semi-multiple states maintains the conducting properties of the system at this particular frequency. The remaining complex fine structures can also be understood according to this simple picture. At semi-multiples of the energy level spacing, distinct classes of photonic excitations will take place in the ac transport processes, giving rise to special transmission features in the diagrams that can only be detected in the presence of magnetic fields.

As a consequence of the semi-multiple excitations found in the case where $\hbar\omega = \Delta/2$, the amplitude and period of FP oscillations shown in fig. 1 will be greatly modified. This can be seen in fig. 5 which presents $V_{bias} \times V_{gate}$ diagrams driven by an ac potential with $V_{ac} = 0.01\gamma_o$ and $\hbar\omega = \Delta/2$ (upper panels) and Δ (lower panels), assuming different B values. For $\hbar\omega = \Delta/2$, the amplitude of the oscillations are less sharp and the characteristic FP diamonds are half the size obtained in fig. 1. In other words, the ac potential blurs the FP patterns, turning the conductance fluctuations less evident. However, when the ac frequency fits the characteristic frequency of the cavity or its integer multiple, $\hbar\omega = n\Delta$, the interference pattern corresponding to the DC case is practically recovered, without missing the diamond line definitions. As B plays its role, a conducting gap and a series of distorted diamonds start to destroy the oscillatory patterns. We can say that the combination of ac and B prompted a new kind of electronic transition engaging semiconducting and FP resonator characteristics whose oscillations can be smoothed out depending on the features of the ac field.

The observed modifications on the electronic response of small CNT radii, as the one investigated here, can only be experimentally detected whether high intensive B is applied. In contrast, the CNTs samples commonly used in the experiments are composed of larger tubes and, consequently, the order of magnitude of B does not overcome 80 T [8]. However, our results can be directly extrapolated for the case of large CNTs samples. The only difference would be that the energy spectrum of the systems would be denser as their diameter increases. When the ac gate acts on the cavity, photonic excitations can be developed, turning the task of discriminating its energy spectrum even more difficult. An alternative way of mapping the energy spectrum of the resonator together with the intermediate photon-induced states is to obtain the conductance modulation when the ac amplitude and B are scanned simultaneously, for a fixed driving frequency, as shown in fig. 6. For the same range of V_{ac}, it is possible to distinguish all the resonant states of the channel for low B intensities. As expected, the spectrum is denser for the driving frequencies smaller than $\Delta/2$ since several sub-multiple photonic states can be induced from the energy splitting $E \to E \pm \hbar\omega$. The resolution of the spectra is gradually damaged as B drives the system towards a semiconducting state.

In summary, we presented a theoretical analysis of carbon-based Fabry-Pérot resonators under the influence of a homogeneous ac-gate plate and an external magnetic field. We demonstrated the possibility of enduring prominent electronic transitions involving semiconducting states induced by the magnetic field and oscillatory conductance patterns. Moreover, depending on the driving frequency, we showed that the periodic profile of the FP patterns can be manipulated. Essentially, the size of the characteristic FP diamonds and the amplitude of the transmission oscillations can be fully controlled with the aid of ac signals. Such a flexible behaviour can be of great use for

the development of ultimately high-frequency field-effect transistors and charge quantum pumping devices.

* * *

This work has received financial support from the Brazilian Agencies CNPq and CAPES, the FAPERJ grants E-26/100.428/2007, and the INCT de nanoestruturas de carbono. AL would like to acknowledge TUD-CNM where part of this work was done for the hospitality. MP would like to acknowledge the Internal Grant USM No. 110971 and FONDECYT No. 1100672. CGR would like to thank the Alexander von Humboldt Foundation.

REFERENCES

[1] Charlier J. C., Blase X. and Roche S., *Rev. Mod. Phys.*, **79** (2007) 677.
[2] Castro-Neto A. H., Guinea F., Peres N. M. R., Novoselov K. S. and Geim A., *Rev. Mod. Phys.*, **81** (2009) 109.
[3] Chen Z. *et al.*, *Science*, **311** (2006) 1735.
[4] Muoth M., Helbling T., Durrer L., Lee S. W., Roman C. and Hierold C., *Nat. Nanotechnol.*, **5** (2010) 589.
[5] Lee S., Lee B.-J. and Shin P. K., *Jpn. J. Appl. Phys.*, **48** (2009) 125006.
[6] Coiffic J. C., Fayolle M., Maitrejean S., Foa Torres L. E. F. and Le Poche H., *Appl. Phys. Lett.*, **91** (2007) 252107.
[7] Liang S. J., Bochrath M., Bozovic D., Hafner J. H., Tinkham M. and Ark H., *Nature*, **411** (2001) 665.
[8] Raquet B., Avriller R., Lassagne B., Nanot S., Escoffier W., Broto J. M. and Roche S., *Phys. Rev. Lett.*, **101** (2008) 046803.
[9] Ritter C., Makler S. S. and Latgé A., *Phys. Rev. B*, **77** (2008) 1954431.
[10] Wakabayashi K., Jujita M., Ajiki H. and Sigist M., *Phys. Rev. B*, **59** (1999) 8271.
[11] Rocha C. G., Latgé A. and Chico L., *Phys. Rev. B*, **72** (2005) 854191.
[12] Latgé A. and Grimm D., *Carbon*, **45** (2007) 1905.
[13] Kohler S., Lehmann J. and Hanggi P., *Phys. Rep.*, **406** (2005) 379.
[14] Foa Torres L. E. F. and Cuniberti G., *Appl. Phys. Lett.*, **94** (2009) 222103.
[15] Zhu R. and Chen H., *Appl. Phys. Lett.*, **95** (2009) 122111.
[16] Prada E., San-Jose P. and Schomerus H., *Phys. Rev. B*, **80** (2009) 245414.
[17] Rocha C. G., Foa Torres L. E. F. and Cuniberti G., *Phys. Rev. B*, **81** (2010) 114535.
[18] Krompiewski S., Martinek J. and Barnas J., *Phys. Rev. B*, **66** (2002) 073412.
[19] Poumirol J. M., Crest A., Roche S., Escoffier W., Goiran M., Wang X., Li X., Dai H. and Raquet B., *Phys. Rev. B*, **82** (2010) 041413.
[20] Nardelli M. B., *Phys. Rev. B*, **60** (1999) 7828.
[21] Rocha C. G., Dargam T. and Latgé A., *Phys. Rev. B*, **65** (2002) 165431.
[22] Tien P. K. and Gordon J. P., *Phys. Rev. B*, **129** (1963) 647.
[23] Orellana P. A. and Pacheco M., *Phys. Rev. B*, **75** (2007) 115427.
[24] Platero G. and Aguado R., *Phys. Rep.*, **395** (2004) 1.
[25] Barone S. R. *et al.*, *Phys. Rev. A*, **15** (1977) 1109.